Received: 21 April 2020 | Revised: 4 June 2020 | Accepted: 5 June 2020

DOI: 10.1002/app.49569

ARTICLE

Applied Polymer SCIENCE WILEY

Nonlinear influences of process parameters on mechanical properties of physically foamed, fiber-reinforced polypropylene parts

Clemens Kastner[1,2] | Georg Steinbichler[1] | Susanne Kahlen[3] | Michael Jerabek[3] | Thomas Lummerstorfer[3]

[1]Institute of Polymer Injection Molding and Process Automation, Johannes Kepler University Linz, Linz, Austria

[2]Competence Center CHASE GmbH, Linz, Austria

[3]Borealis Polyolefine GmbH, Linz, Austria

Correspondence
Clemens Kastner, Johannes Kepler University Linz, Institute of Polymer Injection Molding and Process Automation, Altenbergerstrasse 69, Linz, Upper Austria 4040, Austria.
Email: clemens.kastner@jku.at

Funding information
Österreichische Forschungsförderungsgesellschaft, Grant/Award Number: 868615; Austrian Research Promotion Agency

Abstract

The importance of foam injection molded components in industrial applications increases, above all driven by sustainability concerns. In practice, their applicability almost exclusively depends on their mechanical behavior, which is still difficult to predict based on their microstructure. This work aims to present an approach based upon phenomenological observations. From a processing perspective, the objective is to describe the direct processing-properties-relationship. Therefore, this work focuses on the effects of different processing parameters on selected final mechanical properties of foam injection molded components using glass fiber-reinforced polypropylene. A full factorial, central composite design allows for the detection of nonlinear effects, the application of response surface methodology, and the creation of contour plots. Considering three important process parameters (mold temperature, degree of foaming, delay time) and—for the automotive industry—highly important mechanical properties in bi- and uniaxial bending, the results show a detailed picture of individual dependences, but also two-dimensional interactions between the different process parameters. Improvements of more than 140% in absorbed energy and flexural stiffness were obtained at constant part weight. Modulus and strength were increased by 37 and 44%, respectively.

KEYWORDS

foams, mechanical properties, polyolefins, thermoplastics

1 | INTRODUCTION

Polyolefins are widely used in many areas of application. While the market requirements on final products generally increase, one aspect that attracts more and more attention over the recent years is sustainability.[1,2] Polyethylene and polypropylene[3] are vital components both in terms of economic production and sustainability issues due to their simple, energy-saving production, and processing. Especially in the field of transportation, plastics help to decrease weight and, therefore, to reduce fuel consumption, emissions, and so forth. According to Davies, for instance, a 10% reduction in vehicle weight yields a 5% improvement in fuel economy.[4]

Injection molding is among the most important processing technologies for polymeric materials.[5,6] To keep abreast of imposed requirements, numerous special procedures have been developed, one of them being foam injection molding.[7] This technology can be used to further expand the weight-saving potential of polymeric materials. It facilitates the production of parts with a compact outer layer and a porous core, imitating sandwich components but only consisting of one material.

Its initial purpose upon introduction in the 1950s was the reduction of sink marks. The first serial production of foamed parts for weight reduction took place in the 1970s.[8] Further developments at the Massachusetts Institute of Technology led to the manufacturing of microcellular foams (i.e., average cell sizes between 5 and 100 μm and cell densities greater than 10^9 cells/cm^3).[9] The technology was later licensed by Trexel Inc. (Wilmington, MA) under the trade name MuCell. Nowadays, the technology is used in the automotive industry, for insulation appliances, in construction, the sporting goods industry, or for electronic components like monitor housings.[10–12]

Foam injection molding is based on a dissolved blowing agent in the polymer melt. When the polymer-gas solution enters the cavity, it experiences a pressure drop (i.e., thermodynamic instability) that leads to desorption of the gas and therefore foaming of the polymer. Apart from potential weight saving on the final part, this procedure offers many other advantages. Gas dissolved in the polymer melt reduces the viscosity of the mixture. With CO_2, reductions of more than 50% were achieved.[13–15] In addition, foam injection molded components are easily recyclable (only one constituent), and numerous properties of foamed parts can be improved (e.g., thermal[16,17] or acoustic[18] insulation, shrinkage and warpage[19] behavior, etc.).

Despite many advantages, there are also several drawbacks. Apart from an increased procedural effort, the most severe one is the deterioration of absolute (not relative) mechanical properties (e.g., absolute tensile strength,[20] or modulus[21]) because of the microcellular morphology that is formed during foaming. Therefore, understanding the mechanical behavior of foamed components and its dependence on process management is essential to make full use of the lightweight potential these components offer.

Most studies only focus on two directly interdependent links of the causality chain *Processing-Morphology-Property*, that is, either on the *Processing-Morphology-* or on the *Morphology-Property-relation*. The influence of processing parameters on morphology was studied by Wu et al.,[22] Seo et al.,[23] Zhang et al.[24] or Barzegari and Rodrigue,[25] not taking into account its influence on the mechanical behavior. The morphology-property-relationship, on the other hand, was addressed by Li et al.,[26,27] Fazekas et al.,[28] or Grenestedt et al.,[29] whereas not attaching great importance to processing parameters.

Only a few studies cover the whole causality chain. Matana studied the effect of the foaming conditions on the void fraction, volume expansion ratio, and impact and tensile properties of foamed PLA.[30] They observed a large influence of foaming time and temperature on cell size, void fraction, and volume expansion. Significant improvement of impact behavior but a deterioration of tensile properties was measured. Sun et al. also investigated the impact of foaming time and temperature on cell structure and foam density but focused on tensile and compressive properties.[31] Tovar-Cisneros et al. studied the effect of mold temperature on average cell dimension, cell density, and skin thickness ratio, while also characterizing impact and flexural behavior.[32] Wurnitsch investigated the effect of mold temperature, gas content, and injection speed on morphology and mechanical properties.[33] Feng et al. found that elevated temperatures and foaming time lead to decreased compression modulus and strength in a two-step foaming process, emphasizing the importance of process parameters like mold temperature and delay time.[34] Yet still, a process set up to reach a desired performance profile is barely possible.

The present work is an essential extension of one of our recent works,[35] where the influences of seven process parameters on selected mechanical properties were examined. It was found that mold temperature, degree of foaming (i.e., the opening stroke of the mold; increase of final part thickness) and delay time (i.e., the time between injection of the melt into the cavity and the performance of the mold opening stroke) are the most important in terms of bi- and uniaxial bending behavior. However, the experimental design in this previous work only allowed for the detection of linear dependences. In the present work, the three major process parameters were included in a full factorial, central composite design that permits the identification of nonlinear dependencies. Additionally, two-dimensional interactions could be identified and quantified.

This article is a further step toward tailoring mechanical properties by adjusting selected processing parameters. It is an approach that skips the analysis of morphology and directly forges the bridge between processing and performance. Together with our initial research, this work should offer a guideline for preliminary settings before starting a production and help to understand the relationship between processing and final outcome to make the best use of the advantages of foam injection molding in the most cost-efficient way.

2 | THEORETICAL BACKGROUND

2.1 | Modeling of flexural behavior

Figure 1 schematically shows a foamed bar with a three-layer structure. Core and skin layer possess thicknesses t_c and t_s, respectively, resulting in a total thickness of $t = t_c + 2t_s$. The corresponding densities and Young's moduli of these layers are ρ_c, E_c, ρ_s, and E_s.

The bending stiffness, S_B, can be calculated using Equation (1). Herein, I_c and I_s denote the second moments of area of core and skin layer, calculated according to Equations (2) and (3), respectively. For the calculation of I_s, the parallel axis theorem has to be applied.

$$S_B = E_c I_c + 2E_s I_s = \frac{w}{12}\left[E_c t_c^3 + 2E_s\left(t_s^3 + 3(t_c + t_s)^2 t_s\right)\right], \quad (1)$$

$$I_c = \frac{w t_c{}^3}{12}, \quad (2)$$

$$I_s = \frac{w t_s{}^3}{12} + \left(\frac{t_c + t_s}{2}\right)^2 w t_s. \quad (3)$$

Equation (1) requires knowledge of the Young's modulus of the porous core. According to Avalle et al.,[36] it can be derived from the properties of the solid material (i.e., ρ_s and E_s of the skin layer) and the density of the core, ρ_c, via Equation (4).

$$\frac{E_c}{E_s} \approx \left(\frac{\rho_c}{\rho_s}\right)^2. \quad (4)$$

In this work, the cavity with initial height, t_0, is volumetrically filled before foaming is initiated by mold opening to the final height, t. In this case, Equation (5) allows the calculation of ρ_c.

$$\rho_c = \rho_s \frac{t_0 - 2t_s}{t - 2t_s}. \quad (5)$$

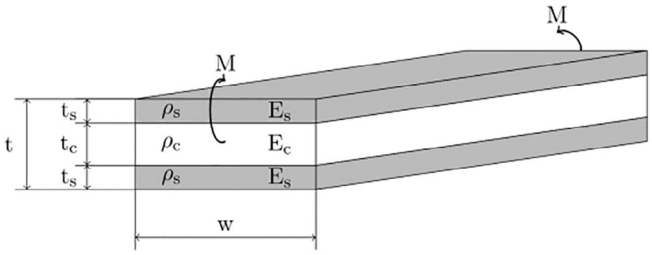

FIGURE 1 Schematic three-layer structure under bending moment

With known Young's moduli of the compact skin layer and the porous core, the bending stiffness can be calculated by combining Equations (1)–(3). The bending stiffness of the entire foamed beam can be expressed by Equation (6), with flexural modulus and second moment of area of the foam, E_f and I_f.

$$S_B = E_f I_f = E_f \frac{w t^3}{12}. \quad (6)$$

As also shown by Johnson and Sims,[37] an expression for the flexural modulus of the foamed beam can be derived from Equations (1) and (6), by defining ν as t_c/t or $(t\text{-}2t_s)/t$:

$$E_f = E_c \nu^3 + E_s\left(1 - \nu^3\right). \quad (7)$$

Equation (8) allows for the calculation of the strain, ϵ, which is present in a distance, z, from the neutral phase of a beam under momentum, M.

$$\epsilon = \frac{M z}{S_B}. \quad (8)$$

The largest strains are acting in the compact layer at $z = t/2$. The failure criterion is the strain, ϵ_u, at which the material fails. This ultimate strain is defined via Hooke's law, with σ_u being the stress at failure. For brittle materials, this stress can be the tensile strength, for ductile materials the yield strength, or any other ultimate stress value.

$$\epsilon_u = \frac{\sigma_u}{E_s}. \quad (9)$$

Combining Equations (7)–(9), the description of the ultimate bearable momentum, M_u, as a function of thickness distribution is possible according to Equation (10). Figure 2 includes a qualitative description of the dependence of the ultimate momentum, M_u, on the thickness of the compact layer, t_s, and total thickness of the foamed beam, t.

$$M_u = \frac{b t^2 \sigma_u E_f}{6E_s} = \frac{b t^2 \sigma_u}{6E_s}\left[E_c\left(\frac{t_c}{t}\right)^3 + E_s\left(1 - \left(\frac{t_c}{t}\right)^3\right)\right]. \quad (10)$$

Together with the linear correlation between momentum and force, this study emphasizes the importance of the three process parameters mold temperature (i.e., skin layer thickness), degree of foaming (i.e., total thickness, morphology), and delay time (i.e., skin layer thickness).

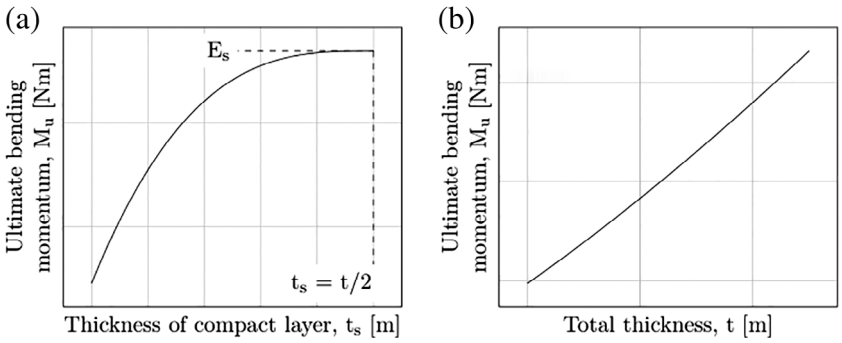

FIGURE 2 Ultimate bending momentum as a function of compact layer thickness (a) and total thickness (b)

3 | EXPERIMENTAL

3.1 | Material

For this work, a 20 wt% short-glass fiber-reinforced polypropylene (PP-GF20) was used as received from Borealis Polyolefine GmbH (Linz, Austria). According to the datasheet, this material is designed for injection molding and is intended for automotive interior applications, which imposes certain mechanical requirements, like good impact behavior and high stiffness, on the material. With a melt flow rate of 12 g/10 min, it is suitable for foaming applications. It exhibits a flexural modulus of 4,200 MPa at a solid density of 1.04 g/cm^3. Nitrogen was used for all foaming trials in this work.

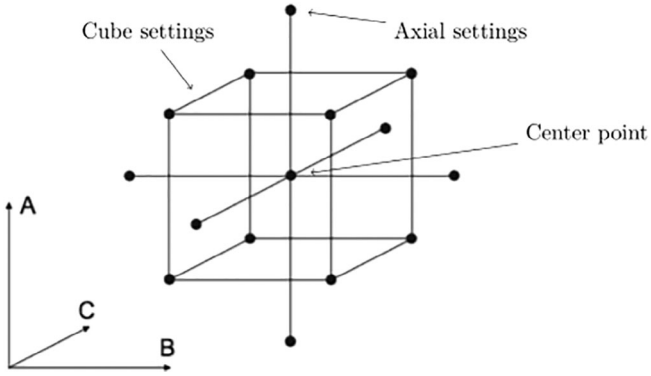

FIGURE 3 Schematic depiction of a full factorial, central composite design

3.2 | Experimental design

Based on the results from our previous work,[35] the three most important process parameters mold temperature, degree of foaming, and delay time should be investigated in more detail. As these previous experiments did not allow for the detection of nonlinear relationships between processing parameters and final mechanical properties, a full-factorial central composite experimental design was created in this work.

This kind of experimental design is based on a regular full factorial design covering two settings for each of the three process parameters (cube). The corners of the cube are formed by the normalized settings ± 1 of each process parameter. This design is extended by six axial points and a center point. The axial points are placed outside the cube and centered over the side of the cube. Therefore, these settings consist of mean settings in between settings ± 1 (Setting 0) of two process parameters and an extreme value of the third one (Setting ±α). The center point in the middle of the cube consists of the mean of all ±1-settings of each parameter. Figure 3 schematically depicts such a central composite design.

The center point setting was realized eight times for an assessment of reproducibility (see chapter "Evaluation of Reproducibility"). All other settings were performed once, resulting in a total of 22 experimental settings.

There were some limitations in terms of absolute levels of process parameters (e.g., a mold temperature below 35°C was not possible). Table 1 includes the settings for each process parameter. The levels of mold temperature represent a trade-off between data-sheet values provided by the supplier and the limitations mentioned above. For the upper levels of the degree of foaming (initial mold height is 2 mm) and delay time, it was important to produce parts of adequate quality, especially at low mold temperature.

All other process parameters were kept constant throughout all experiments. Melt temperature was set to 230°C; gas content was fixed at 0.5 wt%. MuCell-Process-Pressure (i.e., back pressure) and injection speed were set to 120 bar and 50 mm/s, respectively. For statistical evaluation and the creation of contour plots, the software R Project was used in combination with RcmdrPlugin.DoE, an R commander plugin for experimental designs.

TABLE 1 Investigated process parameters and defined levels

Process parameter	Label	Level–α	Level−1	Level 0	Level+1	Level+α
Mold temperature	A	35°C	50°C	60°C	70°C	85°C
Degree of foaming[a] (density reduction)	B	0 mm (0%)	0.3 mm (13%)	0.5 mm (20%)	0.7 mm (26%)	1 mm (33%)
Delay time	C	0.5 s	2 s	3 s	4 s	5.5 s

[a]Opening stroke of the mold.

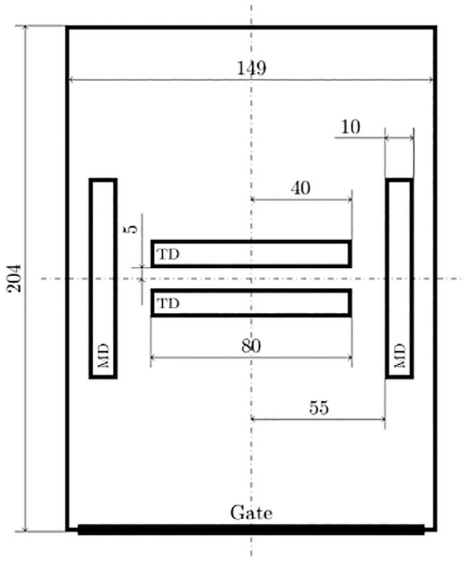

FIGURE 4 Injection molded plaques and position of samples for uniaxial bending tests

3.3 | Sample preparation

All plaques were produced on an e-victory 400/120 injection molding machine (Engel Austria GmbH, Schwertberg, Austria). For gas supply, a MuCell- and an SII-unit (Trexel, Inc., Wilmington, MA) were mounted. A mold without vertical flashes or retractable core was used. The dimensions of the cavity in the closed state are 204 × 149 × 2 mm. The actual foaming process was initiated by opening the mold up to 1 mm according to the experimental design.

For biaxial bending tests, the plaques were used as received from injection molding. Uniaxial bending tests were performed on 10 × 80 × t mm test specimens, with t denoting their final thickness. Specimens in (MD) and transverse to (TD) flow direction were prepared. Due to flow phenomena, MD-specimens exhibit fiber orientation in the longitudinal direction, while fibers in TD-specimens are oriented crosswise. They were milled according to the scheme in Figure 4.

3.4 | Mechanical characterization

A Zwick/Roell ZMART.PRO with a semicircular indenter (diameter 20 mm) and a sample holder with an annular recess (diameter 100 mm) were used for biaxial bending measurements. The samples were not clamped to avoid additional forces and stresses. Vaseline was applied before every test to reduce friction. For a reduction of scattering of the results, the moving speed of the indenter was as low as 10 mm/s. During biaxial bending tests, maximum force, F_{max}, and energy to reach that force, E_{max}, were measured (an assessment of force at initial damage is also provided later). This energy was calculated by the integration of force over displacement. Five specimens per experimental setting were tested.

For the conduction of uniaxial three-point bending tests, a Zwick Z010 with a maximum force of 10 kN and a 500 N load cell for force measurement was used. Radii of indenter and sample holder were 5 mm; the support distance was 46 mm. The test speed was set at 1.2 mm/min in order to reach strain rates in the range of 1%/min at the outer layer, depending on the thickness of specimens. From flexural tests, effective flexural moduli, E_F, and flexural strength, σ_F, were calculated automatically, bending stiffness, S_B, was calculated using Equation (6). Four specimens of each direction (MD, TD) per setting were used for measurements.

The values reported in this work are absolute mechanical properties. All plaques were produced at constant weight per unit area. Standardization with respect to density (i.e., the calculation of relative mechanical properties) was not carried out. This work should reveal the pure influence of the foaming process on the mechanical behavior of foamed plaques.

4 | RESULTS AND DISCUSSION

A summary of all numeric results for bi- and uniaxial bending experiments is provided in Table S1. The table contains the average values of all consecutive measurements within each experimental setting.

TABLE 2 Average values and *SD*s of all center point settings

Mechanical property	F_{max} (N)	E_{max} (J)	$E_{f,MD}$ (MPa)	$E_{f,TD}$ (MPa)	$\sigma_{F,MD}$ (MPa)	$\sigma_{F,TD}$ (MPa)
$\bar{x}_i$	461.7	1.46	3,724	2,129	77.8	49.9
s_i	14.5	0.07	22.42	7.28	0.48	0.22
Percentage (%)	3.15	4.67	0.60	0.34	0.61	0.43

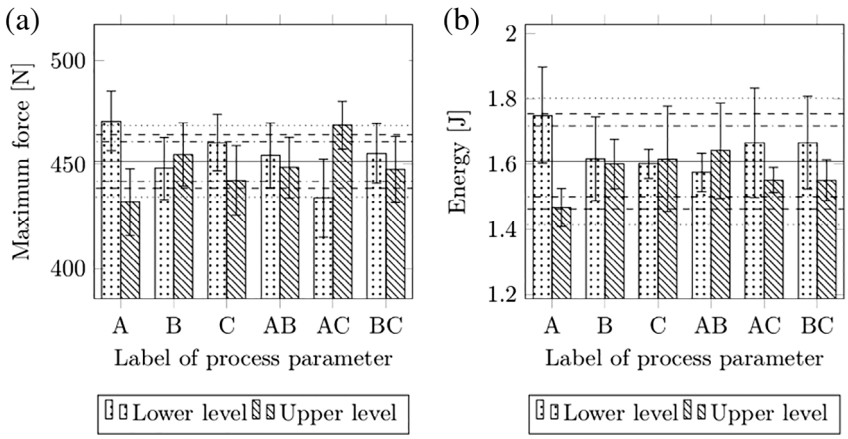

FIGURE 5 Main effect plots for (a) maximum force and (b) biaxial bending energy. Solid line = grand average, confidence intervals: dot-dashed = 99.9%, dashed = 99%, dotted = 95%. Labels of process parameters: mold temperature (a), degree of foaming (b), delay time (c)

4.1 | Evaluation of reproducibility

For an evaluation of reproducibility, the center point (see Figure 3) was covered by eight consecutive experimental runs, each consisting of five (biaxial bending) or four (uniaxial bending) individual measurements. Consequently, 40 samples for biaxial bending, 32 MD-samples, and 32 TD-samples for uniaxial bending were produced at identical process settings. Table 2 summarizes the averages, $\bar{x}_i$, and *SD*s, s_i, for all examined mechanical properties. Flexural stiffness is neglected, as these values correspond with the moduli. No mechanical property exhibits a *SD* of more than 5%, based on the average value. *SD*s for uniaxial bending tests are even under 1%. Reproducibility has, therefore, been confirmed.

4.2 | Biaxial bending tests

Five consecutive measurements are performed at each setting. Averages and *SD*s were evaluated for both maximum force, F_{max}, and total energy, E_{max}. In general, the results for energies scatter slightly more than those for maximum force. The reason for this is the failure behavior of the plaques. Especially at large degrees of foaming (i.e., large final part thicknesses), the maximum force is only reached at large displacements. In these cases, the failure behavior described a "sawtooth" profile. An example is provided in Figure 6. Evaluation of reproducibility within each of the 22 settings shows that F_{max} and E_{max} are out of tolerance in only 2 and 7 settings, respectively (i.e., their *SD* is more than 10% of the average).

A central composite design can be evaluated as a whole or as separate components. As a first step, a statistical analysis of single process parameters and their two-factor interactions under consideration of only the cube settings (see Figure 3) should be conducted. The cube represents an ordinary 2^3 full-factorial design. Figure 5 includes main effect plots for both maximum force and energy. Bars represent averages; error bars describe the *SD*. Table 3 numerically summarizes the results for biaxial bending experiments. It contains the percentage of the difference between the lower (− 1) and upper (+ 1) level setting and the grand average. The stars in Table 3 correspond to the confidence intervals in Figure 5.

An increase of mold temperature from the lower (− 1) to the upper (+ 1) level reduces the maximum force the plaques can withstand by 39.1 N or 8.65%. The corresponding absorbed energy is reduced by 17.59%. Among the experimental settings on the cube, this parameter is the only one having a significant influence on the mechanical properties. All other process parameters only show influences below significance. It is important to note the highly significant effect of the two-factor interaction between mold temperature and delay time. Its positive sign stems from a beneficial combination of low mold temperature and short delay time. The dominant influence of mold temperature agrees with previous measurements.

TABLE 3 Absolute and percentile effects of process parameters and their interactions on maximum force and energy.

Process parameter	Abs. effect on F_{max} (N)	Effect on F_{max} (%)	Abs. Effect on E_{max} (J)	Effect on E_{max} (%)
Mold temperature (A)	**−39.05**	**−8.*** **	**−0.283**	**−17.59***
Degree of foaming (B)	6.69	1.48	−0.016	−1.01
Delay time (C)	−18.20	−4.03	0.015	0.93
AB	−5.80	−1.28	0.067	4.18
AC	35.03	7.76***	−0.114	−7.09
BC	−7.72	−1.71	−0.115	−7.15

Note: Confidence intervals: ***>99.9%; **99–99.9%; *95–99%.
The most significant effects in bold

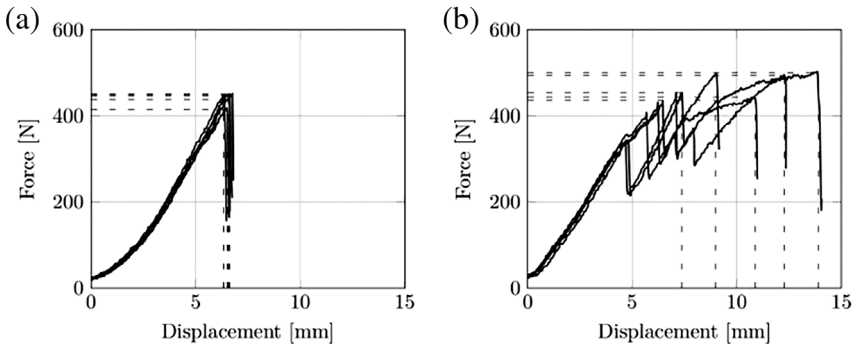

FIGURE 6 Different failure behaviors of plates with (a) minimum (i.e., setting−α) and (b) maximum (i.e., setting+α) degree of foaming. Horizontal dashed lines: maximum forces, vertical dashed lines: bounds of integration for calculation of energy

Since a broader range of parameter settings usually causes larger influences on mechanical properties, the axial and center points were analyzed next. Using the corresponding results (Settings ±α) from Table S1, main effect plots can be created. The plots shown in Figure 7 consist of the ± α-settings and the average of all 0-settings for each process parameter. An increase in mold temperature from 35 to 85°C decreases the maximum force by 5.1% but reduces the absorbed energy by 37.2%. An even larger deviation from the cube settings is measured regarding the degree of foaming. While the maximum force rises by 8.8% when the final plaque thickness is increased from 2 to 3 mm, the energy is more than doubled (+ 140.9%). As mentioned, this behavior can be explained by the failure behavior of the plaques at large degrees of foaming. Figure 6 shows the recorded force-displacement-curves at the ±α-settings for the degree of foaming. As can be seen in Figure 6a, at the lowest degree of foaming (Setting−α), a linear increase of the force up to F_{max} was observed. At the largest degree of foaming (Setting+α), a stepwise failure behavior takes place, as shown in Figure 6b. This shifts the bounds of integration (i.e., the displacement where F_{max} is reached) to the right, thus increases the area under the curves. The large scattering of displacements and simultaneously low scattering of maximum forces at large degrees of foaming explains the worse reproducibility of energy compared to F_{max}. Compared to mold temperature and degree of foaming, the effect of delay time almost vanishes; however, a maximum at a delay time of approximately 3 s can be assumed.

Based on the presented plots, it is possible to find an optimum process setting for the maximization of both force and energy. A component with optimized final mechanical properties made of PP-GF20 should be manufactured at a low mold temperature and a large degree of foaming. Following the argumentation from the Theoretical Background as presented above, a large delay time should also lead to an improvement of mechanical properties as it also increases the skin layer thickness. It is assumed that the reason for the absence of this influence is the presence of a threshold value for this thickness, as a sufficient amount of material has to remain in the core for the foaming process. Therefore, the influence of mold temperature and delay time always depends on other process parameters like initial thickness, thermal conductivity, melt stability of the material, and so forth.

To verify the results, a comparison against the full-factorial cube settings should be drawn. The largest force in biaxial bending tests with 500 N was measured on the cube at low mold temperature (50°C) and a large degree of foaming (i.e., a final part thickness of 2.7 mm). Regarding energy, the second and third largest values on the cube were measured at the same settings (two values because of settings ±1 for delay time). Considering the complete experimental design, the largest energy was obtained at the +α-setting of the degree of foaming (i.e.,

at a final part thickness of 3 mm). This setting also yields a maximum force of 474.2 N, which is in the upper quarter of all results. The lowest energy uptake was measured at the −α-setting (i.e., at a final part thickness of 2 mm), emphasizing the importance of foaming in terms of energy uptake.

The influence of the mold temperature from the axial points is qualitatively comparable to the ones obtained from the full-factorial cube settings; however, its order of magnitude is not. There are two reasons for the strong dissent between results observed on the full-factorial cube and those from the axial points. First, the axial points facilitate the calculation of nonlinear effects of different influencing process parameters. Evident from the plots in Figure 7, many of them show strong curvature. This means that the change in a mechanical property caused by a certain process parameter increases dramatically in one direction while it almost disappears in the other. This behavior can explain the difference in absolute change between cube and axial settings. The region of clear influence was simply not met with the cube settings.

Another reason is interactions between process parameters. The maximum force, for instance, reaches a maximum at a mold temperature slightly below 60°C. An in- or decrease beyond or below that temperature leads to a decline in the final mechanical property. This behavior is at variance with the common explanation that thicker compact layers (i.e., lower mold temperatures) always improve the mechanical behavior. An explanation (apart from sufficient material that needs to be present in the core) could be that the data point at a mold temperature of 60°C comprises the average of the ±α-settings for the other two parameters and also includes the 0-settings. Consequently, this value combines many individual influences and interactions.

Until now, linear influences of single process parameters and their interactions were evaluated using the full-factorial cube design; nonlinear influences were evaluated by means of the axial component of the design. To resolve nonlinear influences of interactions between parameters, contour plots were created based on response surface methodology. These plots are able to represent the combined influence of two process parameters on a selected target property. As this work includes three process parameters, 3 two-dimensional plots have to be created. The third parameter was always kept constant at the 0-level. Figure 8 includes all contour plots for maximum force and energy.

These plots show that interactions between single process parameters are much more complex than one would expect by simply analyzing the main effect plots presented above. Increasing the degree of foaming, for instance, only leads to an increase in maximum force at low delay times. In the covered region, this effect vanishes at prolonged delay times. Further increase of the

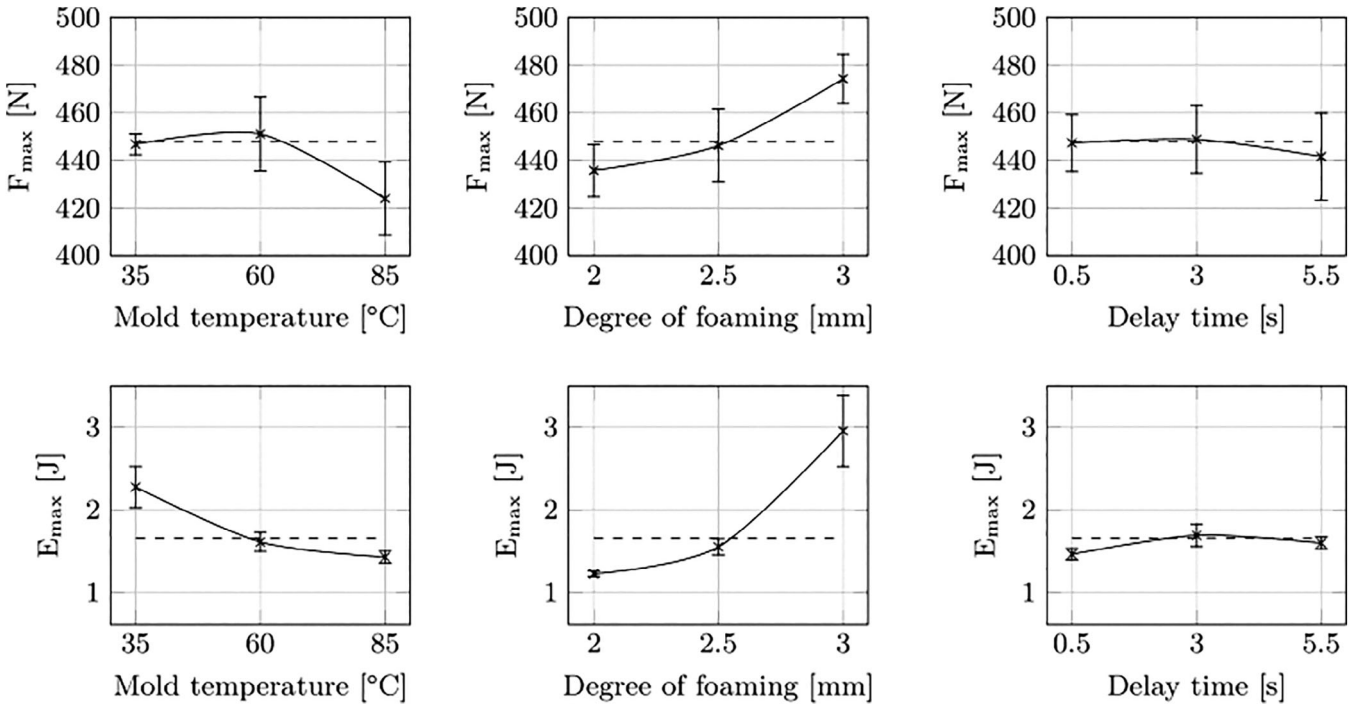

FIGURE 7 Nonlinear main effect plots of maximum force and energy derived from the star points (settings±α) for maximum force (top) and energy (bottom)

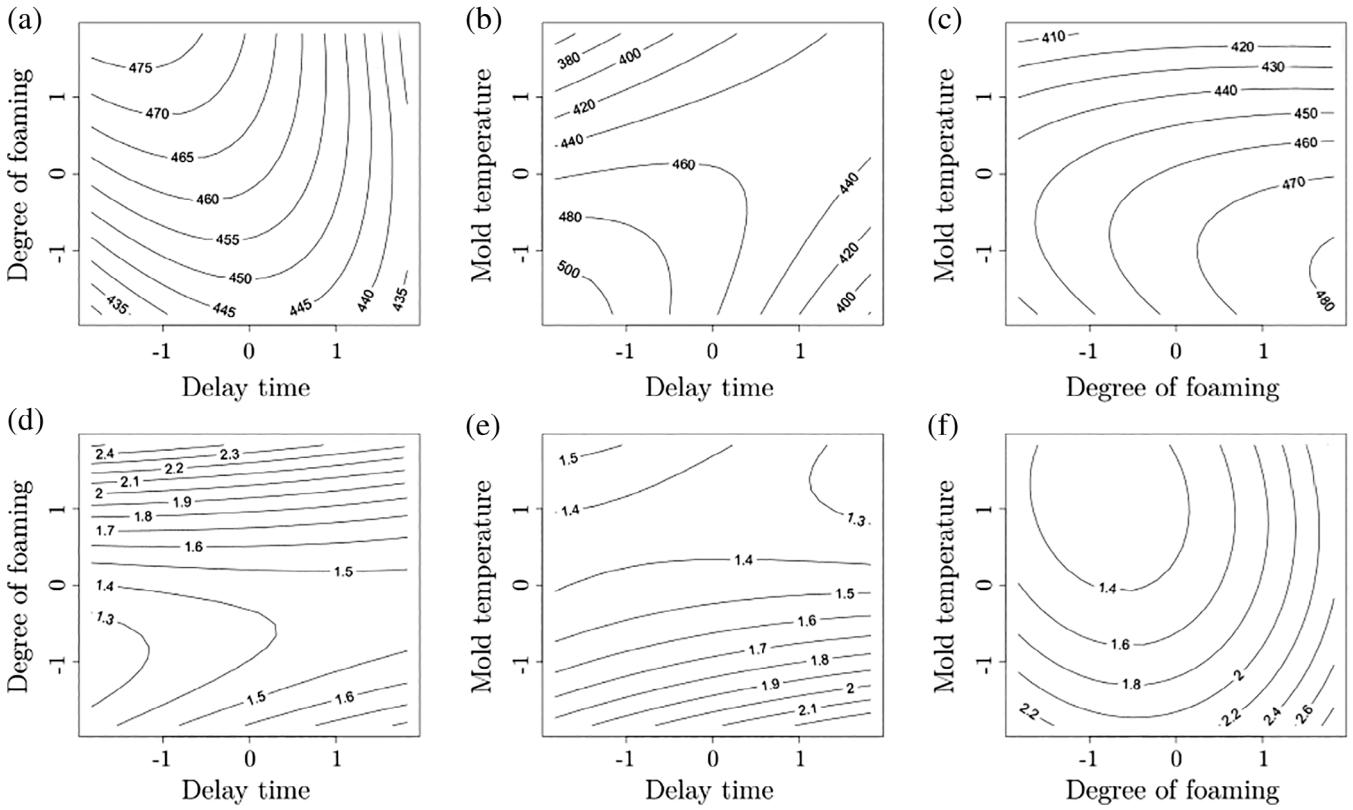

FIGURE 8 Contour plots for visualization of combined influences of two factors on (a)–(c) maximum force and (d)–(f) energy

processing window could even lead to a complete reversal of the effect. The reason for this behavior could be the material distribution inside the plaques. All plaques were produced at a constant weight per unit area. Beyond a certain delay time (i.e., beyond a certain frozen skin layer thickness), the core contains too little material to form a stable foamed core that is capable of transmitting shear forces. As a result, the two compact layers behave similarly to two stacked plaques.

Figure 8a suggests that the maximum force is reached at short delay times and a large degree of foaming (i.e., upper left corner). The need for a low delay time is also shown in Figure 8b. Simultaneously, the mold temperature should be kept low. The necessity of low mold temperature and a large degree of foaming can also be derived from Equations (4) to (7) as a thick compact layer increases the modulus and leads to a smaller decrease with the degree of foaming. The latter also increases the ultimate bearable momentum (see Figure 2). The results for maximum force are self-consistent, and an optimum setting can be found without any contradictions.

For maximizing the absorbed energy also a clear relationship between processing and the final property is found. A large degree of foaming and a low mold temperature lead to higher energy absorption. Only the effect of delay time is not very distinct, as shown in Figure 8d,e.

All heretofore discussed results deal with the ultimate force and the energy that was necessary to pierce through the plaque completely. For many industrial applications, not the ultimate failure, but the initial development of a defect is of interest. This first appearance of a defect can be detected as a first peak in the force-displacement-plots as they were received in this study (an example is provided in Figure 9). Therefore, an analysis regarding the force at the initial formation of damage, F_D, and the corresponding energy, E_D, is conducted. In contrast to analysis up to the complete destruction of the plaques, this study shows a clear relationship between force and energy. Figure 10 shows a linear relationship between force and energy necessary for the formation of a first damage.

Apart from this linear relationship, also the contour plots are qualitatively equivalent, meaning that the three investigated process parameters have the same influences on both force and energy. For that reason, only the plots for the force, F_D, are presented in the following.

The grand average of forces and energies at initial damage lie 7.6 and 21.6% below the ultimate values, but no clear relationship between values at initial damage

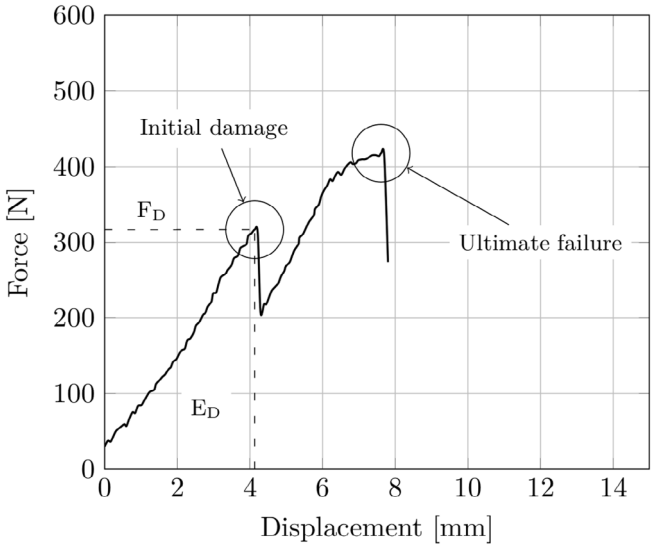

FIGURE 9 Exemplary measurement from cube settings, exhibiting a peak prior to ultimate failure (mold temperature: 70°C, degree of foaming: 0.7 mm, delay time: 2 s)

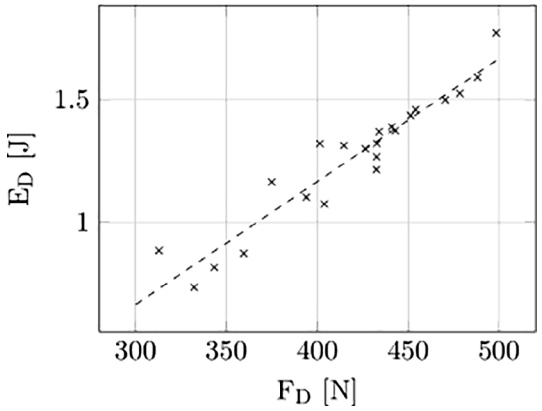

FIGURE 10 Linear relationship between force and energy at initial formation of a damage (dashed: trend line)

and ultimate failure can be observed. The influence of mold temperature and delay time remains unchanged. The same settings as for optimization of maximum force lead to improved behavior. A difference exists in the requirements regarding the degree of foaming, which should be low, according to Figure 11c. This shows that in terms of force and energy at initial damage, it is not possible to find an optimized setting.

4.3 | Flexural tests

The influence of the investigated process parameters on the flexural behavior is more distinct than on biaxial bending behavior. Flexural moduli (therefore, also stiffness) of MD-specimens are, on average, 74% higher than those of TD-specimens. For flexural strength, the difference between specimens in and transverse to flow direction is 55%. Apart from their absolute order of magnitude, MD- and TD-specimens respond to process parameters qualitatively equivalent. For that reason, only the former is discussed in the following. For data analysis, the same procedure, as described above, is applied. First, the cube is analyzed in terms of linear main effect plots. The results are summarized in Figure 12 and Table 4.

By far, the most important process parameter is the degree of foaming. Both flexural modulus and strength deteriorate with an increase of final part thickness. For the modulus, this is in perfect agreement with the behavior predicted by Equation (7). Comparison of mathematically predicted curves and the results from this work show that by fitting only the thickness of the compact layer, $t_{s,calc.}$, it is possible to describe the mechanical behavior of foamed plaques, as shown in Figure 13. The scattering in the y-direction represents interactions between process parameters apart from the degree of

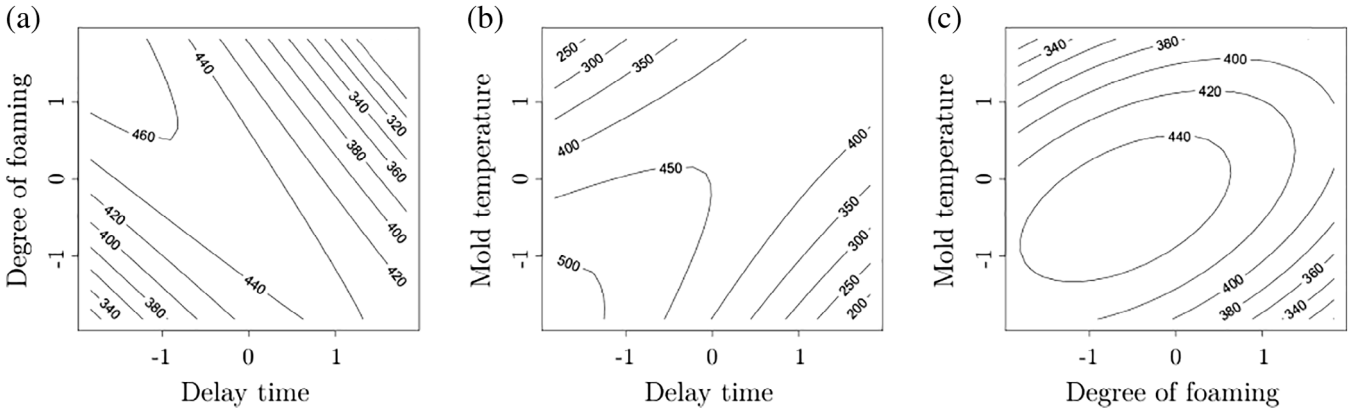

FIGURE 11 Contour plots for visualization of combined influences of two factors on force at initial damage

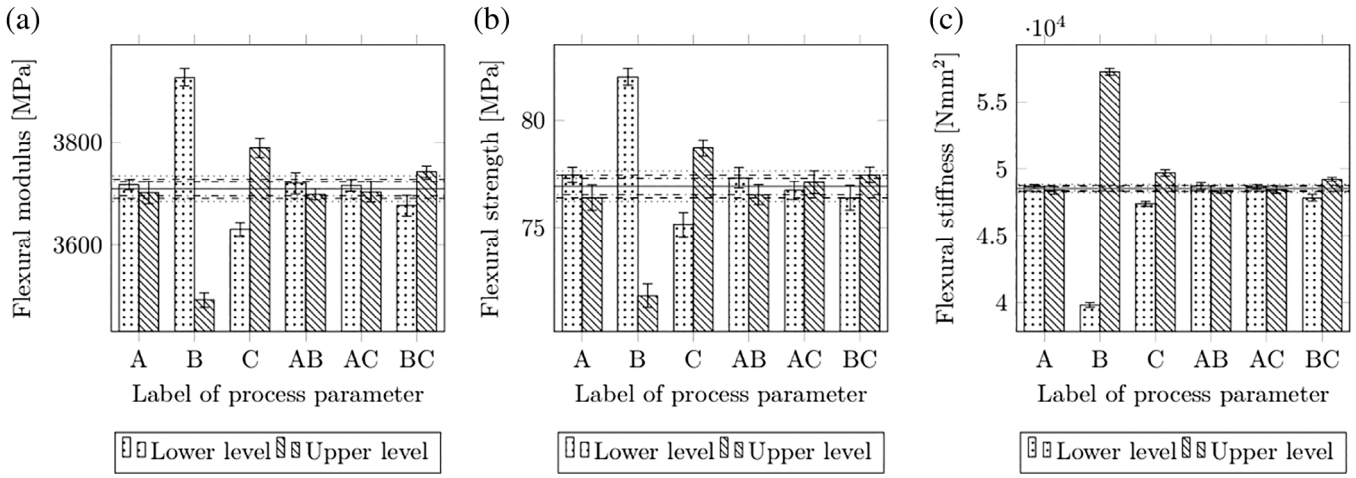

FIGURE 12 Main effect plots for (a) flexural modulus, (b) strength, and (c) stiffness. Solid line = grand average, confidence intervals: dot-dashed = 99.9%, dashed = 99%, dotted = 95%. Labels of process parameters: mold temperature (a), degree of foaming (b), delay time (c)

TABLE 4 Absolute and percentile effects of process parameters and their interactions on flexural modulus, strength and stiffness

	Effect on $E_{F,MD}$		Effect on $\sigma_{F,MD}$		Effect on $S_{B,MD}$	
Process parameters	**(MPa)**	**(%)**	**(MPa)**	**(%)**	**(N mm^2)**	**(%)**
Mold temperature (A)	−15.63	−0.42	−1.05	−1.36**	−273.90	−0.56
Degree of foaming (B)	**−436.13**	**−11.76*** **	**−10.15**	**−13.20*** **	**17,447.66**	**35.94*** **
Delay time (C)	**160.00**	**4.31*** **	**3.57**	**4.64*** **	**2,330.41**	**4.80*** **
AB	−21.25	−0.57	−0.78	−1.02*	−330.94	−0.68*
AC	−12.63	−0.34	0.38	0.49	−198.86	−0.41
BC	**66.13**	**1.78*** **	**1.06**	**1.38****	**1,378.60**	**2.84*** **

Note: Confidence intervals: *** > 99.9%; ** 99–99.9%; * 95–99%.
Most significant effects in bold.

FIGURE 13 Comparison between calculation and measurement of flexural modulus and stiffness

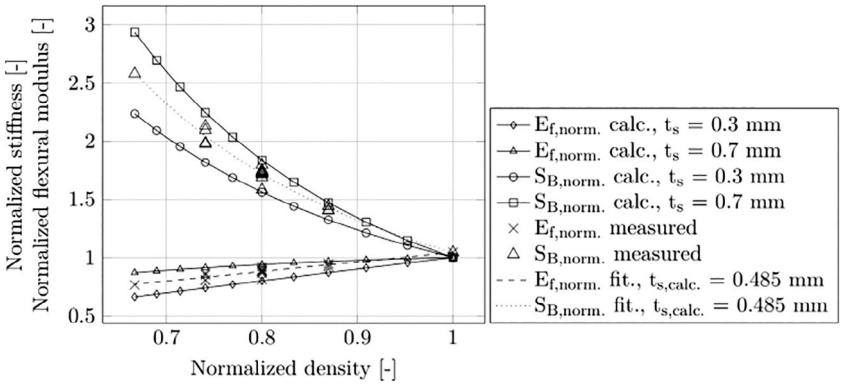

foaming. Compared to the absolute magnitude of measured values, this scattering can effectively be neglected. This result shows that it is possible to eliminate the final thickness as a process parameter from an experimental design when the mechanical behavior of foamed plaques should be examined.

An increase in delay time leads to an improvement in the overall bending behavior. As Figure 2 suggests, a reason for that behavior could be the thicker compact layers. However, as mold temperature does not show any influence on the bending behavior, another parameter besides the thickness of the compact layer is responsible for that influence. Also, its interaction with the degree of foaming has a large effect on bending behavior. Based on findings published in our previous work,[35] it is assumed that a finer cell structure develops with prolonged delay

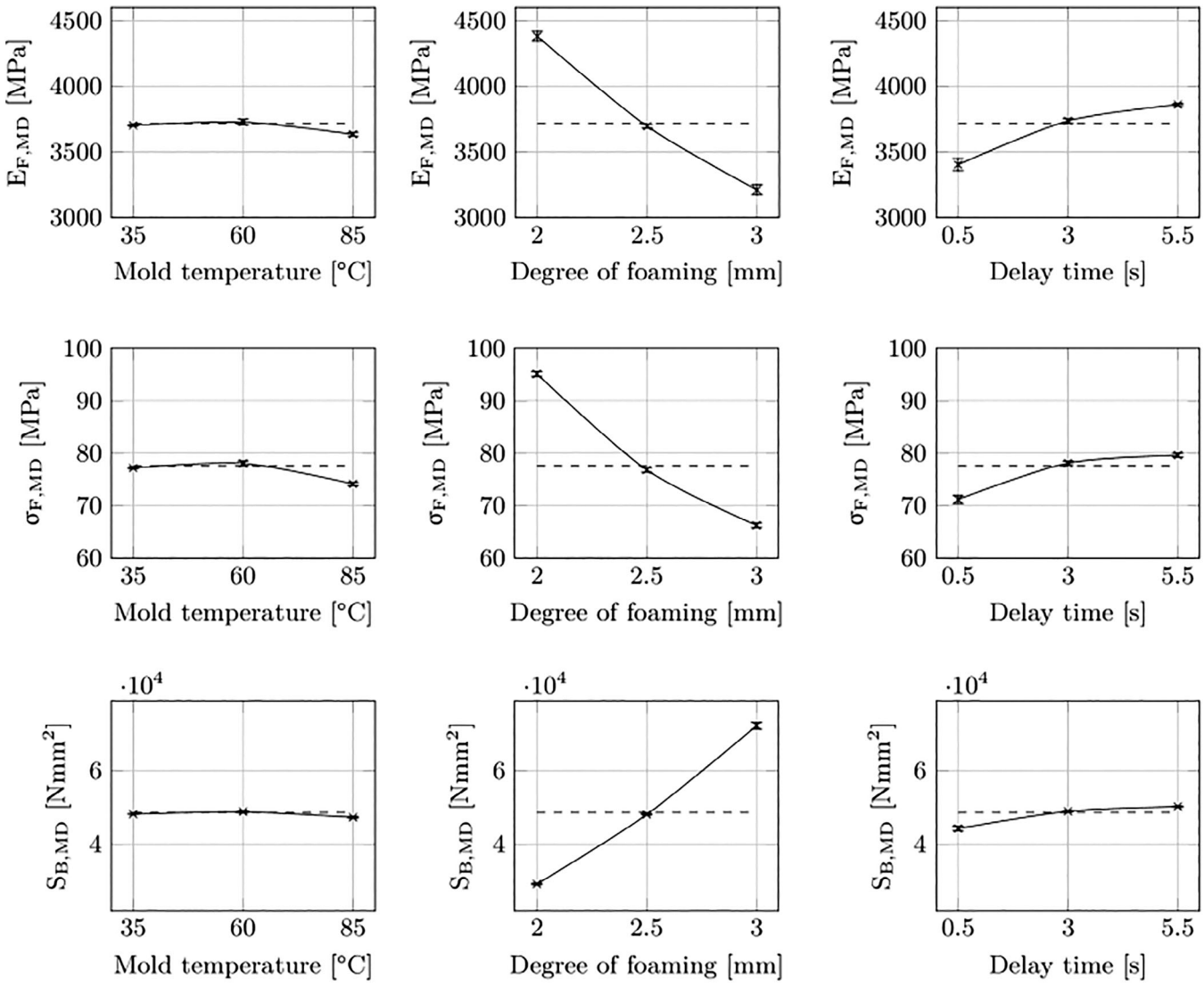

FIGURE 14 Nonlinear main effect plots of maximum force and energy derived from the star points for flexural modulus (top), strength (middle), and stiffness (bottom)

times and that this improves the bending behavior. Further investigations are required.

Nonlinearity should again be inspected by using the axial component of the experimental design. The corresponding results are summarized in Figure 14. As can be seen, the effect of mold temperature is almost inexistent, indicating that the thickness of the compact layer is of little importance. One explanation for that behavior is the mode of loading. In contrast to uniaxial bending, radial tension in the plaques is the predominant load in biaxial bending experiments. Only little shear forces are present. This tensile load can be carried by thick skin layers more easily.

Concerning the degree of foaming and delay time, the results from linear analysis can be confirmed. Between the measured modulus values of settings with the highest and lowest degree of foaming (Experiment no. 14 and 15), a difference of more than 1,000 MPa is observed. The flexural moduli of 3,210 and 4,381 MPa are indeed the largest and lowest measured values in the whole series of experiments. The same is true for flexural strength. An increase of the final thickness from 2 to 3 mm leads to a drop in both modulus and strength by 26.7 and 30.3%, respectively. Stiffness, on the other hand, increases by 147.3%.

The delay time influences all investigated properties positively. Its influence accounts for an improvement of 458 MPa and 5,963 N mm^2 or 13.5% in flexural modulus and stiffness and 8.4 MPa or 11.8% in strength. It is assumed that the foam structure is responsible for this behavior. Due to the prolonged , the material is hindered from foaming, the gas nucleates more homogeneously and forms a finer cell structure, which obviously improves uniaxial bending behavior. In summary, the

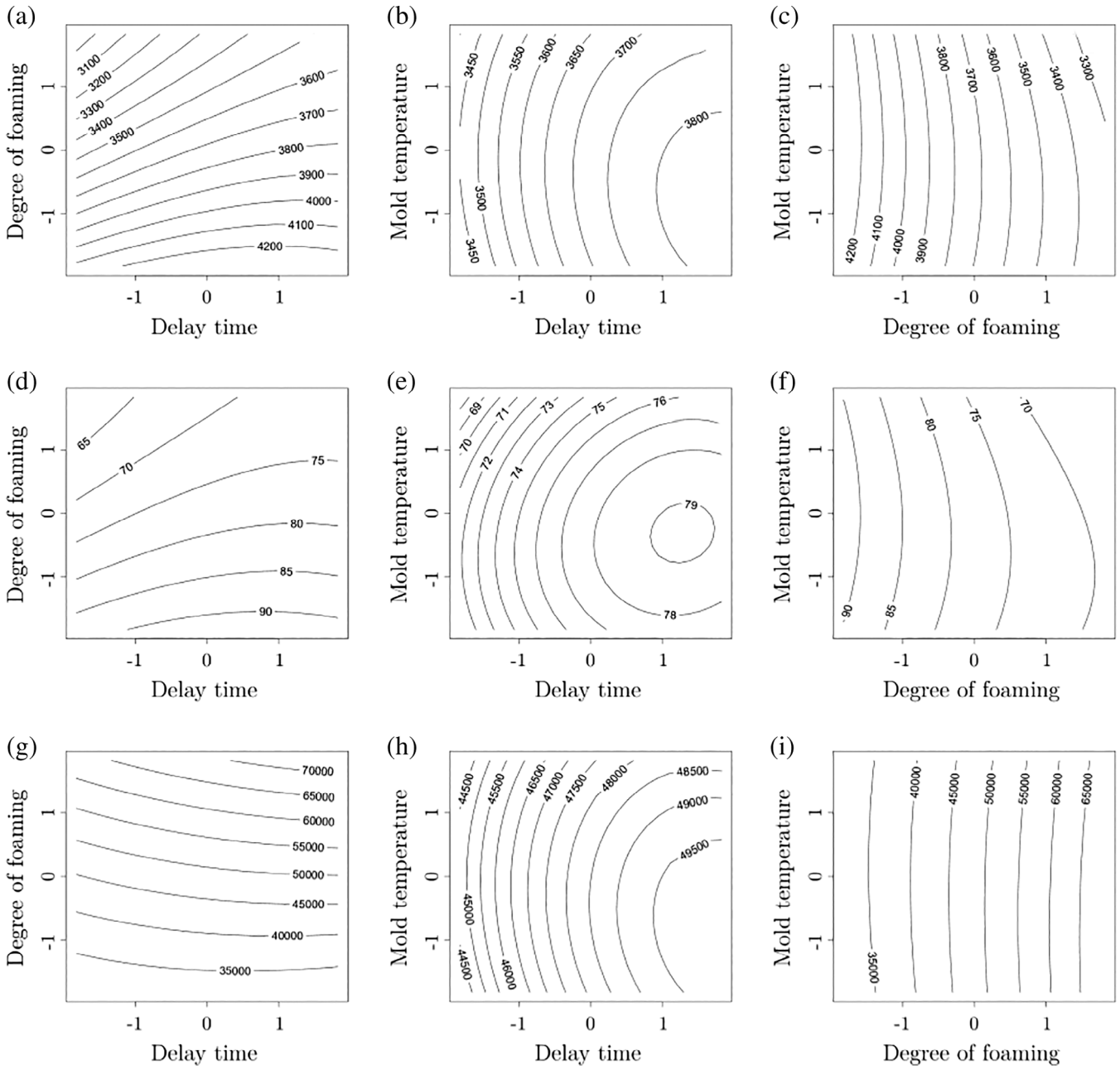

FIGURE 15 Contour plots for visualization of combined influences of two factors on flexural modulus (top), strength (middle), and stiffness (bottom)

uniaxial bending behavior in terms of modulus and strength is maximized by a low mold temperature and degree of foaming and long delay time. Flexural stiffness is only influenced by the degree of foaming. An optimization of modulus, strength, and stiffness at the same time is not possible due to conflicting demands on the degree of foaming.

Utilizing the complete experimental design, it is again possible to create contour plots, as summarized in Figure 15. The shape of the contour lines is qualitatively equivalent for all mechanical properties. Fewer interactions than for the biaxial bending behavior can be observed. In general, the flexural modulus benefits from a low degree of foaming. In the covered area, an almost linear relationship between this process parameter and the mechanical behavior was determined. Interestingly, the mold temperature only affects the flexural behavior (in terms of modulus, strength, and stiffness) at long delay times. In this region, an optimized setting is found to be located around the 0-setting. Mold temperatures beyond and below that value lead to a decrease in the investigated mechanical properties. As

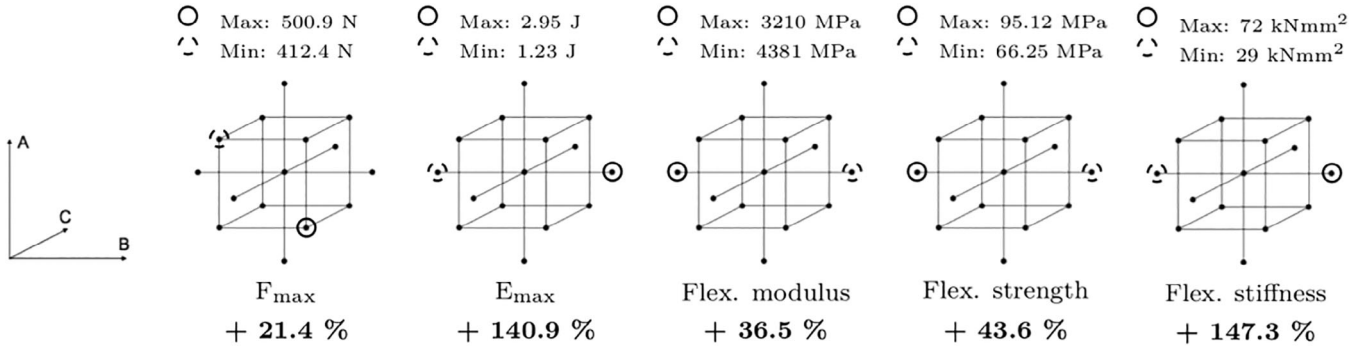

FIGURE 16 Best and worst mechanical properties and their position on the experimental design (numbers below give the improvement within the DOE)

observed in our previous work, the mold temperature significantly influences the foam structure. It was observed that higher mold temperatures lead to finer cell structures. It is assumed that at longer delay times, the material is given enough time to form a fine structure at a mold temperature of roughly 60°C. Beyond that temperature, the core of the plaque solidifies too slowly, leading to the coalescence of cells. Larger cells deteriorate the material's ability to carry shear forces that are necessary to transfer tensile forces to the stiff skin layers. Following the argumentation of Equation (4), a mold temperature below the 0-setting could also lead to a poor foam structure, as the nucleation rate is reduced instantly. Regarding all interactions between the three investigated process parameters and their influence on uniaxial bending behavior, it can be concluded that the degree of foaming is of the highest importance. In combination with this process parameter, the influence of the other two vanishes.

5 | CONCLUSIONS

In this work, the influence of three process parameters (i.e., mold temperature, degree of foaming, delay time) on selected mechanical properties is investigated. Two important loading cases are considered: biaxial and uniaxial bending. Interactions between process parameters are much more present at biaxial bending. For the uniaxial loading case, primarily the degree of foaming is influencing the mechanical behavior. Figure 16 summarizes the findings of this work. It includes the largest and lowest values for all investigated mechanical responses and illustrates the position of the setting on the experimental design.

Based on the results from this work, the largest potential of the foaming technology is the improvement of bending stiffness and total absorbed energy, when using PP-GF20. Both properties can be increased by more than 140% when increasing the final part thickness from 2 to 3 mm. Also, the maximum force in biaxial bending experiments or flexural modulus and strength can be improved by more than 20, 30, and 40%, respectively.

All plaques were produced at constant shot weights. These improvements of mechanical behavior are, therefore, only reached by changing process parameters. This implies that no additional costs for larger amounts of material, additional tooling, and so forth are involved. This work clearly shows the huge potential the foaming technology offers in terms of the maximization of mechanical properties while not increasing the expenses during production.

Drawbacks still include some contradictions in terms of the setting for certain process parameters. Concerning force and energy at the initial formation of damage, the degree of foaming should be selected high in combination with low delay time but low in combinations with low mold temperature. In uniaxial bending, it is not possible to increase modulus, strength, and stiffness simultaneously. The degree of foaming has a contrary influence on the former two than on the latter.

Another issue that remains is the trade-off between good mechanical behavior and surface appearance. Especially regarding biaxial bending (and supposedly also tensile) behavior, a low mold temperature should be chosen. For obtaining parts with good surface appearance, a high mold temperature is more suitable as it allows a smoothening of the rough surface.

ACKNOWLEDGMENTS

This work was performed within the Competence Center CHASE GmbH, funded by the Austrian Research and Promotion Agency (grant number 868615). The authors acknowledge financial support through the COMET Centre CHASE (project No 868615), which is funded within the framework of COMET – Competence Centers for

Excellent Technologies by BMVIT, BMDW, the Federal Provinces of Upper Austria and Vienna. The COMET program is run by the Austrian Research Promotion Agency (FFG). The financial support and the provision of equipment by companies Borealis Polyolefine GmbH and Engel Austria GmbH is greatly acknowledged. Gratitude is especially owed to Georg Grestenberger, T. L., Daniela Mileva, Dieter Nicolussi, Christof Wurnitsch, and Wolfgang Kienzl for their professional and technical support but also for their administrative aid.

ORCID

Clemens Kastner https://orcid.org/0000-0002-7375-9021

REFERENCES

[1] H. Lewis, K. Verghese, L. Fitzpatrick, *Packag. Technol. Sci.* **2010**, *23*, 145.
[2] A. Gallego-Schmid, J. M. F. Mendoza, A. Azapagic, *Sci. Total Environ.* **2018**, *628-629*, 979.
[3] J. M. Eagan, J. Xu, R. Di Girolamo, C. M. Thurber, C. W. Macosko, A. M. LaPointe, F. S. Bates, G. W. Coates, *Science* **2017**, *355*, 814.
[4] G. Davies, in *Materials for Automobile Bodies* (Ed: G. Davies), Butterworth-Heinemann, Oxford, UK **2012**, p. 309.
[5] S. Koltzenburg, M. Maskos, O. Nuyken, *Polymere: Synthese, Eigenschaften und Anwendungen*, Springer, Berlin, Heidelberg **2014**.
[6] H.-P. Heim, *Specialized Injection Molding Techniques*, Elsevier Inc, Oxford, UK **2016**.
[7] F. Johannaber, W. Michaeli, *Handbuch Spritzgießen*, Hanser, Munich **2004**.
[8] A. Handschke, J. Mitzler, *Kunstst. Int.* **2012**, *10*, 151.
[9] X. Xu, C. B. Park, in *In Injection Molding, Technology and Fundamentals* (Eds: M. R. Kamal, A. Isayev, S. J. Liu), Hanser Publications, Munich, Germany **2009**, p. 273.
[10] D. Scherzer, in *Leichtbau in der Fahrzeugtechnik* (Ed: H. E. Friedrich), Springer Vieweg, Wiesbaden (DE) **2013**, p. 443.
[11] M. Altan, in *In Polymerization* (Ed: N. Çankaya), IntechOpen, London, UK **2018**, p. 117.
[12] M. Rohleder, F. Jakob, in *In Specialized Injection Molding Techniques* (Ed: H.-P. Heim), Elsevier, Oxford, UK **2015**, p. 53.
[13] X. Qin, M. R. Thompson, A. N. Hrymak, A. Torres, *Ind. Eng. Chem. Res.* **2006**, *45*, 2734.
[14] M. Lee, C. B. Park, C. Tzoganakis, *Polym. Eng. Sci.* **1999**, *39*, 99.
[15] L. J. Gerhardt, C. W. Manke, E. J. Gulari, *Polym. Sci. B Polym. Phys.* **1997**, *35*, 523.
[16] J. Zhao, Q. Zhao, L. Wang, C. Wang, B. Guo, C. B. Park, G. Wang, *Eur. Polym. J.* **2018**, *98*, 1.
[17] G. Wang, J. Zhao, L. H. Mark, G. Wang, K. Yu, C. Wang, C. B. Park, G. Zhao, *Chem. Eng. J.* **2017**, *325*, 632.
[18] B. Neyciyani, S. Kazemi Najafi, I. Ghasemi, *J. Appl. Polym. Sci.* **2017**, *134*, 45096.
[19] A. Kramschuster, R. Cavitt, D. Ermer, Z. Chen, L.-S. Turng, *Polym. Eng. Sci.* **2005**, *45*, 1408.
[20] S. Wong, J. W. S. Lee, H. E. Naguib, C. B. Park, *Macromol. Mater. Eng.* **2008**, *293*, 605.
[21] L. M. Matuana, C. B. Park, J. J. Balatinecz, *Polym. Eng. Sci.* **1998**, *38*, 1862.
[22] Q. Wu, N. Zhou, D. Zhan, *Plast. Technol. Eng.* **2009**, *48*, 851.
[23] J. H. Seo, W. S. Ohm, S. H. Cho, S. W. Cha, *Plast. Technol. Eng.* **2011**, *50*, 1399.
[24] P. Zhang, N. Zhou, B. Li, *Plast. Technol. Eng.* **2007**, *46*, 885.
[25] M. R. Barzegari, D. Rodrigue, *Polym. Eng. Sci.* **2009**, *49*, 949.
[26] K. Li, X. L. Gao, G. Subhash, *Int. J. Solids Struct.* **2005**, *42*, 1777.
[27] K. Li, X. L. Gao, G. Subhash, *J. Mech. Phys. Solids* **2006**, *54*, 783.
[28] A. Fazekas, R. Dendievel, L. Salvo, Y. Bréchet, *Int. J. Mech. Sci.* **2002**, *44*, 2047.
[29] J. L. Grenestedt, F. Bassinet, *Int. J. Mech. Sci.* **2000**, *42*, 1327.
[30] L. M. Matuana, *Bioresour. Technol.* **2008**, *99*, 3643.
[31] H. Sun, G. S. Sur, J. E. Mark, *Eur. Polym. J.* **2002**, *38*, 2373.
[32] C. Tovar-Cisneros, R. González-Núñez, D. Rodrigue, *J. Cell. Plast.* **2008**, *44*, 223.
[33] C. Wurnitsch, *Diploma Thesis*, Montanuniversität Leoben (Austria) **2001**.
[34] J. M. Feng, W. K. Wang, W. A. Yang, B. H. Xie, M. B. Yang, *Plast. Technol. Eng.* **2011**, *50*, 1027.
[35] C. Kastner, G. Steinbichler, S. Kahlen, M. Jerabek, *J. Appl. Polym. Sci.* **2019**, *136*, 47275.
[36] M. Avalle, G. Belingardi, A. Ibba, *Int. J. Imp. Eng.* **2007**, *34*, 3.
[37] A. F. Johnson, G. D. Sims, *Composites* **1986**, *17*, 321.

SUPPORTING INFORMATION

Additional supporting information may be found online in the Supporting Information section at the end of this article.

How to cite this article: Kastner C, Steinbichler G, Kahlen S, Jerabek M, Lummerstorfer T. Nonlinear influences of process parameters on mechanical properties of physically foamed, fiber-reinforced polypropylene parts. *J Appl Polym Sci*. 2020;e49569. https://doi.org/10.1002/app.49569